ACS NANO

XXXXX XX, XXXX VOLUME XX NUMBER XX

pubs.acs.org/acsnano

Defining nanoscience and nanotechnology

ACS Publications
Most Trusted. Most Cited. Most Read.

www.acs.org

ACSNANO

www.acsnano.org

ARTICLE

Robust Acute Pancreatitis Identification and Diagnosis: RAPIDx

Qingfu Zhu,[#] Jiaxin Luo,[#] Hui-Ping Li,[#] Wen Ye,[#] Reguang Pan, Ke-Qing Shi, Rui Yang, Hao Xu, Hengrui Li, Luke P. Lee,* and Fei Liu*

Cite This: https://doi.org/10.1021/acsnano.3c00922

Read Online

ACCESS | Metrics & More | Article Recommendations | Supporting Information

ABSTRACT: **The occurrence of acute pancreatitis (AP) is increasing significantly worldwide. However, current diagnostic methods of AP do not provide a clear clinical stratification of severity, and the prediction of complications in AP is still limited. Here, we present a robust AP identification and diagnosis (RAPIDx) method by the proteomic fingerprinting of intact nanoscale extracellular vesicles (EVs) from clinical samples. By tracking analysis of circulating biological nanoparticles released by cells (*i.e.*, EVs) via bottom-up proteomics, we obtain close phenotype connections between EVs, cell types, and multiple tissues based on their specific proteomes and identify the serum amyloid A (SAA) proteins on EVs as potential biomarkers that are differentially expressed from AP patients significantly. We accomplish the quantitative analysis of EVs fingerprints using MALDI-TOF MS and find the SAA proteins (SAA1-1, desR-SAA1-2, SAA2, SAA1-2) with areas under the curve (AUCs) from 0.92 to 0.97, which allows us to detect AP within 30 min. We further realize that SAA1-1 and SAA2, combined with two protein peaks (5290.19, 14032.33 *m*/*z*), can achieve an AUC of 0.83 for classifying the severity of AP. The RAPIDx platform will facilitate timely diagnosis and treatment of AP before severity development and persistent organ failure and promote precision diagnostics and the early diagnosis of pancreatic cancer.**

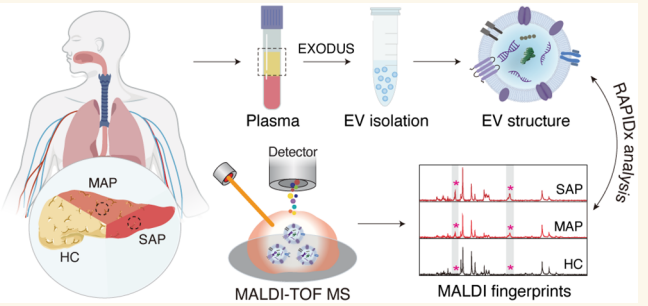

KEYWORDS: *extracellular vesicles, exosomes, acute pancreatitis diagnosis, proteomics, protein fingerprints*

INTRODUCTION

Acute pancreatitis (AP) is characterized by a local and systemic inflammatory response and is the most common gastrointestinal disease requiring acute admissions.[1] The global incidence of AP is estimated to be 33.74 cases per 100,000 persons, with a mortality rate of 1.60 per 100,000 persons.[2] Most patients with mild acute pancreatitis (MAP) can recover completely after proper treatment. However, approximately 20% of patients develop moderate or severe acute pancreatitis (SAP), with a high risk of pancreatic necrosis or organ failure, leading to a substantial mortality rate of 20−40%.[1,3−5] The current diagnostic tests for AP patients relying on biochemical and radiologic evidence, either by serum amylase and lipase testing or imaging studies, are limited by the lack of a standardized reference range and the poor sensitivity of imaging modality in the early stages.[1−3] Contrast-enhanced CT for AP diagnosis is costly and may lead to discomfort or even aggravation of the patient's condition.[4] Moreover, difficulties in prompt identification and clear stratification of the disease severity pose enormous challenges to clinical diagnosis and timely treatment.[5] Therefore, rapid AP detection approaches with reliable biomarkers, especially noninvasive markers enabling precision diagnosis of AP and stratification of its severity, are essential in changing the situation.[6]

Extracellular vesicles (EVs) are nanoscale bioparticles, mainly including exosomes (30−150 nm) and microvesicles (150−1000 nm), secreted by all types of living cells. EVs, especially small EVs (30−200 nm), play essential roles in intercellular communications and participate in various pathological processes such as tumorigenesis, cancer metastasis, and inflammation by delivering active cargoes to recipient cells.[7−9] These EV-carried cargoes, including DNAs, RNAs, proteins, metabolites, and lipids, can be potential biomarkers for many diseases.[7,10−13] The inflamed pancreas also actively releases EVs, which can enter the peripheral blood circulation carrying disease-related information.[14] Moreover,

Received: January 31, 2023
Accepted: March 15, 2023

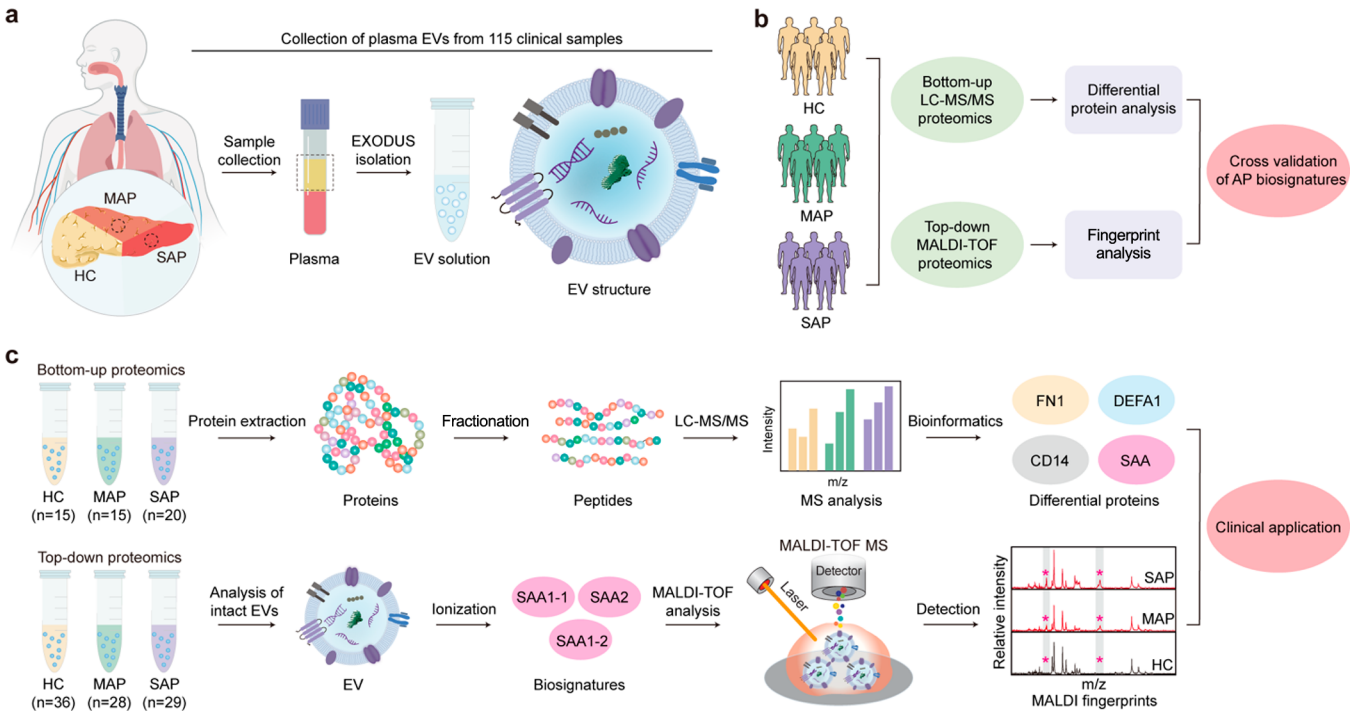

Figure 1. Rapid and high-precision biomarker discovery and acute pancreatitis (AP) diagnosis via circulating extracellular vesicles (EVs). (a) Isolation of circulating EVs released from pancreatitis in patients' plasma. (b) Combining bottom-up proteomics and MALDI-TOF mass spectrometry-based protein fingerprinting analysis to detect and validate AP biosignatures. (c) Workflow of label-free bottom-up proteomics and protein fingerprinting analysis via MALDI-TOF mass spectrometry for AP diagnosis toward clinical applications. HC, healthy control; MAP, mild acute pancreatitis; SAP, severe acute pancreatitis.i

tracking experiments reveal that circulating exosomes can reach the alveolar compartment and are involved in AP-associated lung damage.[15] As a snapshot of physiological status, EVs offer potential insights into AP diagnostics at the early point before cellular necrosis. Recent studies have revealed that EVs are involved in AP-associated organ damage and could mediate AP pathogenesis and propagation.[14,16,17] Thus, investigation of circulating EVs from peripheral blood provides a promising avenue for quantitative diagnosis of AP.

Many platforms have been developed to study EVs for clinical application. The traditional methods, including ultracentrifugation and polymer-based precipitation, are incompatible with a rapid clinical screening test.[13,18] To overcome these limitations, analytical techniques such as acoustofluidic-based vesicle analysis and microfluidic platforms have been reported to facilitate point-of-care applications.[19−21] In addition, the nanoscope imaging platform using microsphere arrays to characterize nanomaterials shows excellent potential for nanoscale EV identification.[22] Our group has recently developed an exosome detection method *via* the ultrafast-isolation system (EXODUS) using nanoporous membrane-based resonators, which can fast-purify EVs from diverse biofluid samples with high purity toward clinical translations.[23] With regard to high-throughput detection platforms, matrix-assisted laser desorption/ionization time-of-flight mass spectrometry (MALDI-TOF MS) has been demonstrated as a powerful analytical tool for quantitatively detecting and analyzing biomolecules such as peptides and proteins.[24,25] Its high sensitivity and throughput allow the rapid detection of molecules over a broad mass range.[26,27] Moreover, the recent applications of MALDI-TOF MS have been extended to evaluate fingerprints of EVs for sensitive cancer diagnostics, either determining fingerprints of proteins from lysed vesicles or fast depicting fingerprints of the whole intact vesicles.[27−29] The EV fingerprinting approach features fast detection and dynamical monitoring of disease status, which allows us to detect disease biomarkers by analyzing the corresponding fingerprint spectra quantitatively, and thus is preferably feasible for clinical applications.

In this work, we develop Robust Acute Pancreatitis Identification and Detection (RAPIDx) based on proteomics fingerprinting of the intact small EVs isolated from plasma samples of patients via the ultrafast-isolation system and MALDI-TOF mass spectrometry. The bottom-up proteomic study has been applied first to profile and track the origins of EV proteins circulating in the plasma of patients with AP and healthy controls. This is to provide biological evidence for applying circulating EVs as disease biomarkers, and another is to discover the characteristic proteins in response to AP initiation and progression. We then demonstrate RAPIDx for fast detection and selection of AP biosignatures. The RAPIDx system allows the speedy isolation of EVs from plasma with high yield and purity, and high-throughput interrogation of EVs in their intact forms omits additional preparation steps such as protein extraction and digestion.[30] We found that EV-carried proteins, especially SAA and its isomers, were significantly differentially expressed between AP and healthy individuals and can be applied as potential markers for AP diagnostics. The established RAPIDx method is rapid and ultrasensitive, which can detect AP from 20 μL of patient plasma within 30 min, providing a feasible way for precision molecular diagnostics of AP toward clinical translations.

https://doi.org/10.1021/acsnano.3c00922
ACS Nano XXXX, XXX, XXX−XXX

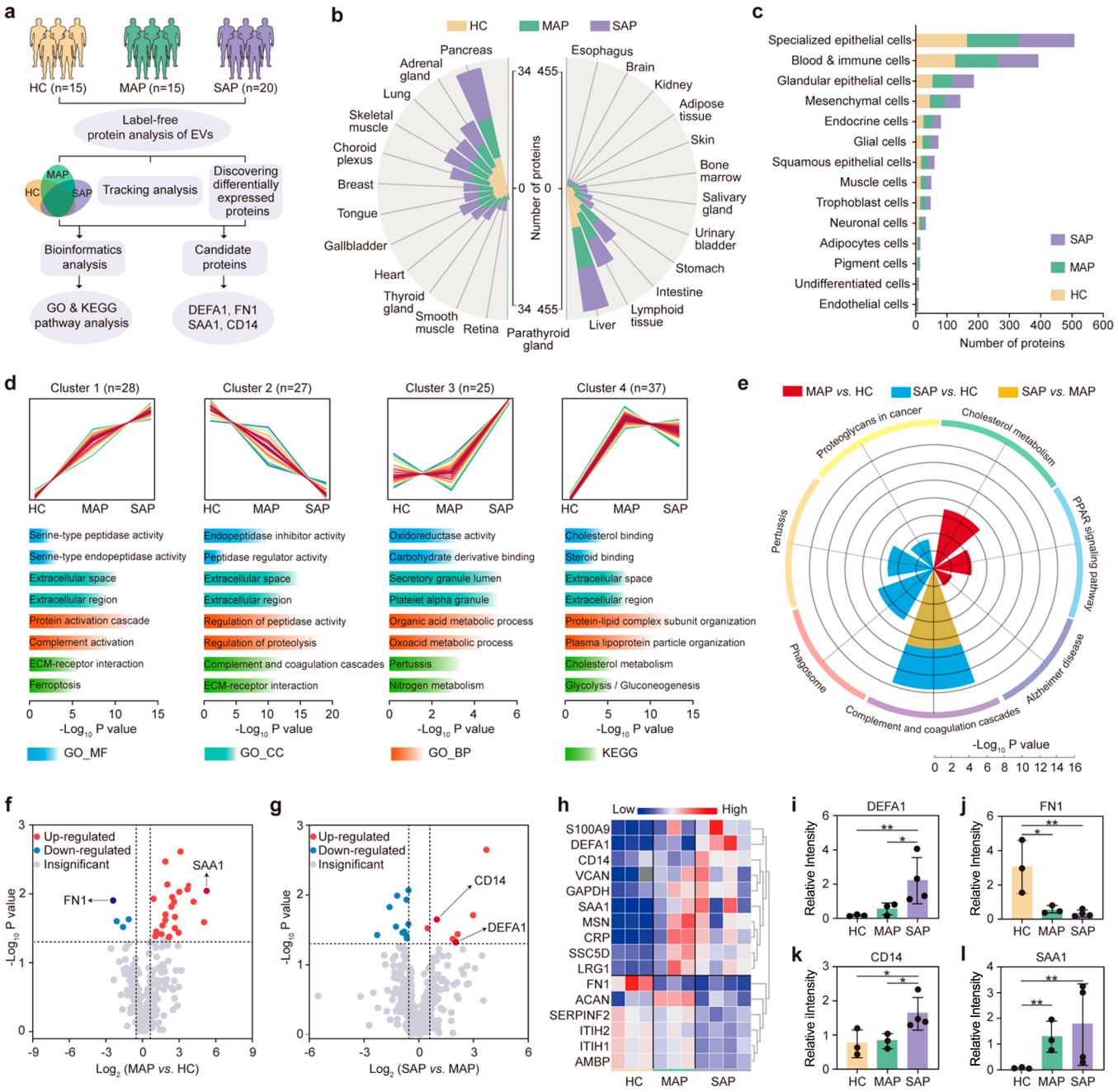

Figure 2. Investigation of potentials of EV proteins as biomarkers for acute pancreatitis diagnosis. (a) The analytical workflow of label-free EV proteomics. HC, healthy control; MAP, mild acute pancreatitis; SAP, severe acute pancreatitis. (b) Protein tracking analysis of identified proteins showing circulating EVs have close phenotype connections to various tissues based on their specific proteomes. (c) Protein tracking analysis of EV proteins for their cell-type origins. (d) Enrichment analysis of proteins in different clusters classified by Mfuzz from all identified proteins. GO, Gene Ontology; MF, Molecular Function; CC, Cellular Composition; BP, Biological Process. KEGG, Kyoto Encyclopedia of Genes and Genomes. (e) KEGG pathway analysis using differential proteins from the following comparisons: MAP *vs.* HC, SAP *vs.* HC, and SAP *vs.* MAP. (f) Volcano plot showing the distributions of differential proteins between HC and MAP, and (g) MAP and SAP. The up-regulated proteins are shown in red; the down-regulated proteins are shown in blue, and the gray dots represent nonsignificant proteins. The differential proteins were selected with a fold change >1.5 and a *P*-value <0.05. (h) Heatmap of all groups crossed differential proteins from the following comparisons: MAP *vs.* HC, SAP *vs.* HC, and SAP *vs.* MAP. (i) The most differentially expressed protein presented in cluster 1, and in cluster 2 (j), and cluster 3 (k), and cluster 4 (l), sorted by their FC values. The protein expression levels of HC, MAP, and SAP groups were compared (**P-value < 0.01, *P-value < 0.05).

RESULTS

Analysis of EVs from the Plasma Samples of AP Patients. The diagnosis of MAP and SAP was primarily investigated as there are urgent clinical needs to detect them precisely and rapidly. AP patients were diagnosed according to the revised Atlanta classification and definitions. The detailed clinical information is shown in Table S1. Figure 1 shows the schematic illustrations of the work design. First, the 115 plasma samples were obtained by centrifuging peripheral blood at 1500*g* with two cycles to avoid contaminations from the

https://doi.org/10.1021/acsnano.3c00922
ACS Nano XXXX, XXX, XXX−XXX

platelet. We isolated and purified EVs from plasma samples *via* EXODUS (Figure 1a).[23] Figure 1b demonstrates the concept of combining the top-down and bottom-up proteomics for discovering AP biosignatures, and the detailed steps have been described in Figure 1c. Before proteomic analysis, the obtained EV samples were evaluated by nanoparticle tracking analysis (NTA), Western blot (WB) analysis, and transmission electron microscopy (TEM) according to the guidelines of the International Society for Extracellular Vesicles (ISEV).[31] Most particles are distributed in a size range of 30 to 200 nm with a peak size of 105 nm (Figure S1a), and the particle size is shown in Figure S1b, which follows the size range of small EVs.[7] The vesicles also show the expressions of EV positive protein markers (CD9, Flot-1) (Figure S1c) and a typical cup-shaped EV morphology (Figure S 1d), indicating the excellent quality of the isolated EV product. The Mac-2BP, a family of beta-galactoside binding proteins associated with the immune response, was also highly expressed on EVs. We then performed EV proteomics with the bottom-up strategy using label-free LC-MS/MS and determined fingerprints of intact EVs using MALDI-TOF MS to investigate and detect potential AP markers.

Bottom-Up EV Proteomics for Protein Tracking Analysis and Biosignature Discovery. We performed bottom-up proteomics with the label-free protein analysis strategy to discover EV origins and evaluate potential EV protein markers (Figure 2a). The EV proteins were extracted and cleaved into peptides for LC-MS/MS analysis. A total of 479 proteins were identified using Proteome Discoverer (Table S2). First, we performed protein tracking analysis and calculated the number of EV proteins mapped to tissues/cells based on their specific proteomes to reveal connections between phenotypes. The data suggest the leading related tissues are the liver, lymphoid, and the tissues involved in the digestion system, including the intestine, stomach, and pancreas (Figure 2b). Further investigating the cell-type sources, we found that the proteins of EVs were mainly related to blood and immune cells (such as T cells, macrophages, monocytes, and plasma cells) and the specialized epithelial cells, the later primarily derived from hepatocytes (liver cells) and also contributed by ductal cells (pancreas cells) and proximal tubular cells (kidney cells) (Figure 2c, Figure S2). Tracking analysis of EV proteins leads to the conclusion that the origin of plasma EVs is closely related to the immune and digestive systems. They may serve as a snapshot of the physiological and pathological status of the corresponding functional parts.

In EV proteome profiles, we observed 419 shared proteins in the tested groups (MAP, SAP, and HC group). Eight and 16 specific proteins of MAP and SAP and 34 shared AP-specific proteins were observed, respectively (Figure S3a). The corresponding enrichment analysis shows that EV proteins of SAP were mainly involved in the metabolism process and regulation of lyase activity, such as small molecule catabolic process, carbon metabolism, and lyase activity. At the same time, MAP and SAP shared proteins (excluding proteins in the HC group) were mainly related to the protein catabolic process, including threonine-type endopeptidase activity, proteasome, proteasomal protein catabolic process, and regulation of proteolysis (Figure S3b–d).

We next compared the overall protein expression levels of the shared proteins from three groups in a heatmap clustered using a complete-linkage method, which reveals the patterns of each group and reflects the potential signatures for AP diagnostics (Figure S3e). We classified the protein expressions into 8 specific patterns using the Mfuzz method to show the dynamic alternations of expression levels between HC, MAP, and SAP groups (Figure 2d, Figure S4). The proteins involved in clusters 1 and 2 are continuously up-regulated and down-regulated, respectively, from HC to MAP and the SAP group (Figure 2d). They are mainly from the extracellular space and are primarily associated with ferroptosis, ECM-receptor interaction, protein activation cascade, proteolysis regulation, and peptidase activity. The expression level of proteins in cluster 3 experiences a relatively continuous period from HC to MAP, and then increases dramatically at SAP (Figure 2d). Thus, the involved proteins in this cluster might be investigated as potential markers for distinguishing SAP patients from HC and MAP. Cluster 4 might be the source of features for differentiating AP from the HC group, as the included proteins show an apparent up-regulating trend from HC to AP (Figure 2d). These proteins were related to metabolic processes, protein–lipid complex subunit organization, and plasma lipoprotein particle organization.

We further investigated the differentially expressed proteins within the shared proteins from HC, MAP, and SAP groups (Figure S5a). They used the selecting criteria of fold change (FC) > 1.5 and *P*-value < 0.05; we obtained differential proteins from the comparisons of MAP *vs.* HC, SAP *vs.* HC, and MAP *vs.* SAP. The resultant enriched pathways based on differential proteins are listed in Figure 2e. The complement and coagulation cascades pathway has been recently reported to be associated with acute necrotizing pancreatitis.[32] There were 29 and 53 differential proteins for MAP and SAP compared to the HC group shown in Figure 2f and Figure S5c, respectively. The corresponding differential proteins are ranked by their FC values in Figure S5b and Figure S5d. It is clearly shown that the SAA1 carried by circulation EVs were the most up-regulated proteins for both MAP and SAP groups compared to the HC group, with up-regulation folds of 37.7 and 51.4, respectively, indicating a robust discriminatory power for AP detection. Comparing the MAP and SAP groups, we identified 17 differentially expressed proteins, as shown in Figure 2g. The top differential proteins of SAP are ITGA2B, CPA1, S100A8, CFHR1, and DEFA1, with FC values ranging from 3 to 13, shown in Figure S5e. These proteins might be strongly correlated with AP severity.

To investigate the dynamic alternations of AP severity, we compared the expression levels of differential proteins across three groups. Figure 2h shows all crossed differential proteins from the following comparisons: MAP *vs.* HC, SAP *vs.* HC, and MAP *vs.* SAP. Combined with the cluster analysis in Figure 2d, we identified the 4 most differential proteins sorted by their FC values in each cluster. Their expression intensities across 3 groups are listed in Figure 2i–l. DEFA1 in cluster 1 and CD14 in cluster 3 potentially served as biomarkers for detecting SAP from MAP and HC. They appeared to be up-regulated proteins in SAP compared to other groups. FN1 in cluster 2 and SAA1 in cluster 4 might be the potential biosignatures for differentiating HC and AP patients. In contrast to SAA1, FN1 appeared as a significantly down-regulated protein in AP compared to HC. By enrichment analysis, we found that the enriched GO terms from the differential proteins of AP were intensively involved in the acute-phase response and acute inflammatory response, such as high-density lipoprotein particles, the innate immune response, and regulation of

https://doi.org/10.1021/acsnano.3c00922
ACS Nano XXXX, XXX, XXX–XXX

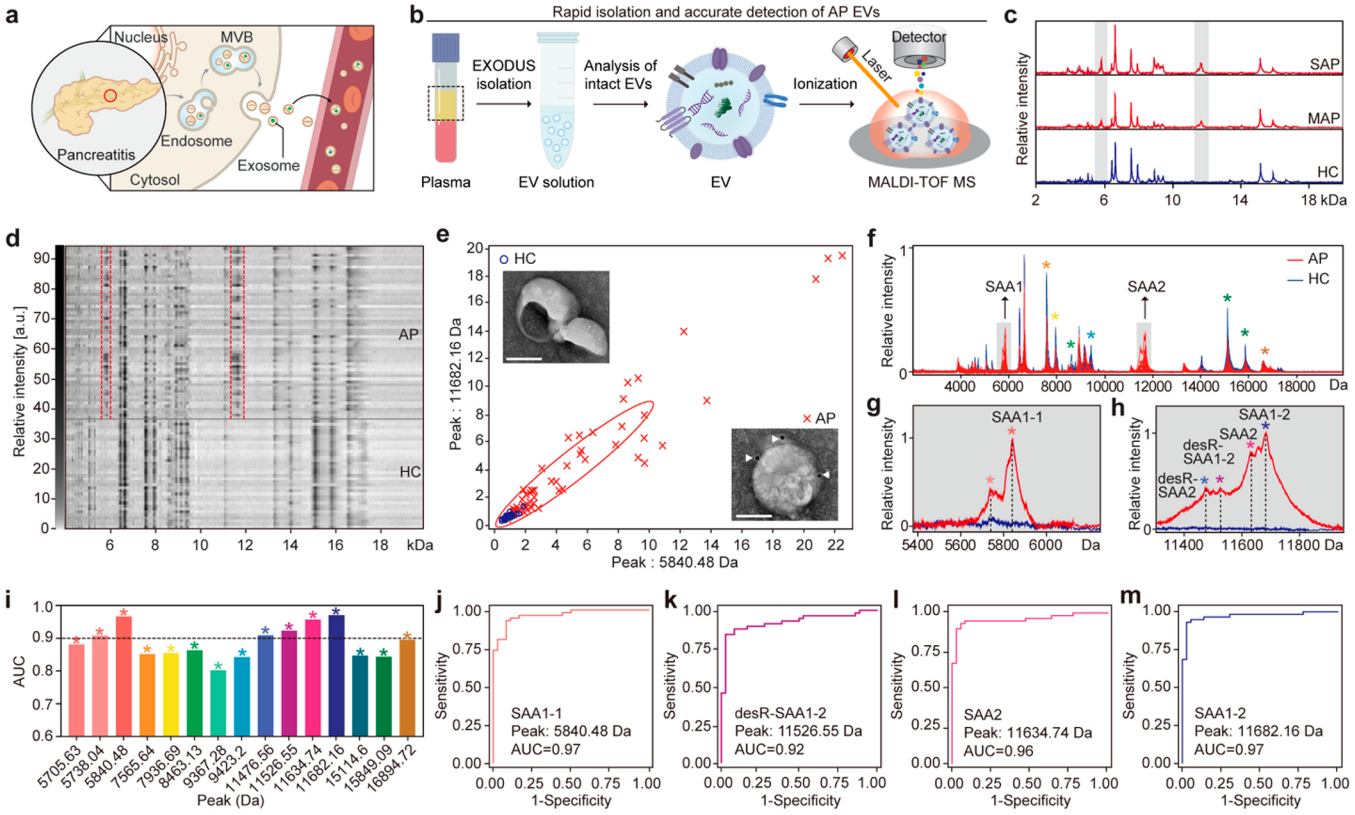

Figure 3. Rapid and accurate identification of acute pancreatitis by RAPIDx. (a) Schematic illustration of EVs released from pancreatitis cells and circulation in blood. (b) Purification of plasma EVs followed by integrated RAPIDx analysis. (c) Protein fingerprints of EVs from HC, MAP, and SAP groups via MALDI-TOF MS analysis. The differentially expressed protein clusters are highlighted in gray. (d) Virtual gel graph of mass spectra of EVs isolated from AP and healthy donors, ranging from 20 to 20000 Da. The specifically expressed protein clusters are highlighted between red lines. The samples were collected from 57 AP patients and 36 healthy individuals. (e) Two-dimensional peak distribution of pancreatitis patient (red circle) and healthy control (blue cross) EVs. The *x*-axis and *y*-axis represent the relative intensity of samples at peaks of 5840.48 (SAA1) and 11682.16 (SAA1-2) Da, respectively. The immunoelectron microscopy analysis was performed against SAA proteins, and the white arrows indicated anti-SAA antibody-labeled gold particles. Scare bar: 50 nm. (f) The overall sum of the spectra obtained from pancreatitis patient (red) and healthy control (blue) samples. The gray area in the figure marks the discriminating peaks, including SAA1 in (g) and SAA2 in (h). (i) Area under the receiver operator characteristic curve for the top 15 discernible mass peaks in the spectra. The receiver operating characteristics (ROC) curves and area under the curve (AUC) values of (j) SAA1-1, (k) desR-SAA1-2, (l) SAA2, (m) SAA1-2 to distinguish pancreatitis patients and healthy controls.

proteolysis (Figure S6a−c). Enriched pathways based on the differential proteins between MAP and SAP were mainly related to response to lipopolysaccharide, blood microparticle, glycosaminoglycan binding, and complement activation (Figure S6d−e). These pathways are close to the immune response, inflammatory response, and pathogenesis and may reflect the initiation and development of AP.

In summary, the applied quantitative proteomics analysis allows the profiling of EV proteins circulating in the plasma of AP patients and discovering EV-related biosignatures for AP diagnosis, providing vital information for understanding pathogenesis and promoting biomarker discovery.

Rapid and Precise Detection of Acute Pancreatitis by RAPIDx. In this work, we demonstrated the capability of RAPIDx for screening the characteristic proteins of AP via analysis of fingerprints of the intact EVs isolated from the plasma samples of patients (Figure 3a−b). The differential peaks of the fingerprints can directly reflect the potential biosignatures of AP groups (Figure 3c). The virtual gel graph of the mass spectra from the AP and HC groups based on the relative expression of proteins is shown in Figure 3d. Overall, each mass spectrum consisted of approximately 52 discernible mass peaks from the groups of AP and HC (Table S3). Compared to the healthy controls, the gel graph of AP patients had two additional bands (marked with red dashed lines in Figure 3d), which could be the specific proteins enriched in the EVs of AP patients. The two-dimensional distribution of each sample based on the two differentially expressed proteins (5840.48 and 11682.16 Da) is plotted in Figure 3e. The AP and control groups show distinct distributions. These two peaks were identified as SAA1 proteins (SAA-1 and SAA1−2) based on their m/z values from reported results.[33,34] This strongly follows the bottom-up proteomics data, which indicated that SAA-1 was the most up-regulation protein of the AP group compared to HC. We further performed immuno-electron microscopy to cross-validate SAA expressions on the EV surface. The anti-SAA antibody labeled gold particles tended to surround vesicles from AP patients instead of HC individuals (Figure 3e, Figure S7). The differentially expressed peaks were also observed in the stacked spectra of all samples (Figure 3f−h). We then compared the discriminatory power of the two groups by calculating the area under the curve (AUC) of the receiver operator characteristic (ROC) curve for the top 15 discernible mass peaks in the spectra, as shown in Figure 3i and Figure S8. Peaks of 5840.48, 11526.55, 11633.74, and 11682.16 Da (m/z) have the highest

https://doi.org/10.1021/acsnano.3c00922
ACS Nano XXXX, XXX, XXX−XXX

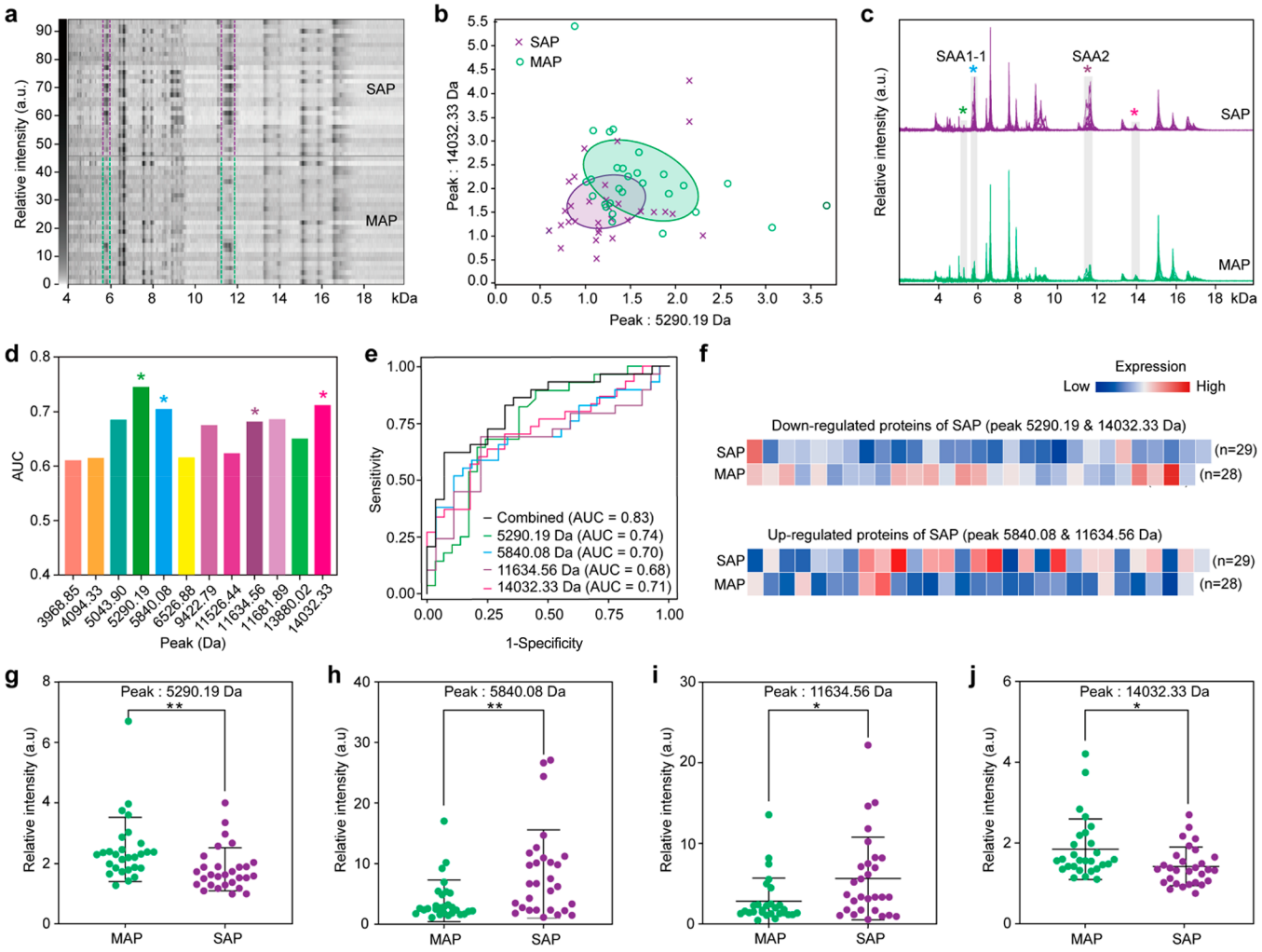

Figure 4. Stratification of acute pancreatitis severity by RAPIDx. (a) Virtual gel graph of mass spectra of EVs isolated from MAP and SAP patients, ranging from 20 to 20000 Da. The significantly differentially expressed protein clusters for the SAP and MAP groups are highlighted between purple and green lines, respectively. (b) Two-dimensional peak distribution of SAP patients (purple cross) and MAP patients (green circle). The *x*-axis and *y*-axis represent the relative intensity of samples at peaks of 5290.19 and 14032.33 Da, respectively. (c) The overall sum of the spectra was obtained from the SAP (purple) and MAP group (green) samples. And the distribution of the mass spectra of significantly different peaks in the SAP and MAP groups is shown, including 5290.19, 5840.08 (SAA1-1), 11634.56 (SAA2), and 14032.33 Da: *X*-axis, mass-to-charge ratio, *y*-axis, relative intensity. (d) The area under the curve (AUC) of peaks is used for classification in the Genetic Algorithm (GA) algorithm model. (e) The receiver operating characteristics (ROC) curves and AUC values of peak 5290.19, 5840.08 (SAA1-1), 11634.56 (SAA2), and 14032.33 Da to distinguish the severity of acute pancreatitis. (f) Heat map showing the expression of peak 5290.19, 5840.08 (SAA1-1), 11634.56 (SAA2), and 14032.33 Da in all test samples, and their intensity comparisons between MAP group and SAP group are shown in (g), (h), (i), and (j), respectively (*P*-value < 0.01, **P*-value < 0.05).**

discriminatory powers (AUC > 0.92), corresponding to the proteins of SAA1 cluster 1 (SAA1-1), desR-SAA-1 cluster 2 (desR-SAA-1-2), SAA2, and SAA1 cluster 2 (SAA1−2). The ROCs for these peaks in distinguishing AP patients from healthy controls are plotted and shown in Figure 3g−h, in which their AUCs range from 0.92 to 0.97. In addition, the differential peak of 13297.62 Da of AP was identified as S100A9 according to reported spectra positions,[33] and the up-regulation trend was consistent with previous bottom-up proteomics (Figure S5, Figure S9). SAA1 was still the most differentially expressed protein for distinguishing the AP and HC groups with the highest AUC. SAA2 was detected with an excellent AUC of 0.96 for diagnosing AP from HC by RAPIDx, which was also a characteristic protein of the AP group from bottom-up proteomics (Figure 3l, Figure S10). The precisely cross-validated results of the SAA signatures for AP detection indicate the excellent accuracy of the RAPIDx detection system. Thus, we expect high-accuracy AP diagnostics to be achieved by simultaneously targeting the alternations of SAA expression levels on circulating EVs through RAPIDx.

We next performed severity-related analysis and observed differentially detected peaks in the mass spectra by dividing AP patients into two groups based on severity, *i.e.*, the SAP and MAP groups. Each mass spectrum consisted of 47 discernible mass peaks (Table S4). From the virtual gel graph of mass spectra (Figure 4a), the differential expression of EV SAA1 from SAP patients was detected (labeled with red dashed lines) compared to that with MAP. The MAP and SAP can be further classified into two clusters based on the two differentially expressed proteins (5290.19, 14032.33 *m*/*z*), as shown in Figure 4b. From the stacked spectra of AP patients (Figure 4c), we found 4 peaks that had a significant intensity

https://doi.org/10.1021/acsnano.3c00922
ACS Nano XXXX, XXX, XXX−XXX

difference in the SAP group, including 2 up-regulated proteins (SAA1-1, SAA2) and two down-regulated proteins (5290.19, 14032.33 m/z). Among the top 12 peaks involved in the statistical model, SAA1-1, 5290.19, and 14032.33 m/z had the highest discriminatory power with AUCs of 0.70, 0.74, and 0.71, respectively (Figure 4d), indicating the statistical difference between the two groups. Using the combination of 4 peaks to distinguish SAP and MAP, we obtained an excellent AUC of 0.83, revealing that these proteins are promising biomarkers for identifying AP severity (Figure 4e). We further investigated the global expressions of up-regulated and down-regulated proteins across all samples, and distinct expression patterns were observed between MAP and SAP, shown in Figure 4f. The corresponding intensity comparisons of these 4 individual markers between the two groups are presented in Figure 4g–j, demonstrating good potential predictive values with the P-values below 0.05.

Taken as a whole, the fingerprints of the intact EVs show great potential for fast discrimination of AP by detecting characteristic peaks with a special focus on SAA proteins. The integrated RAPIDx offers a sensitive and quantitative detection method for diagnosing acute pancreatitis by analyzing biosignatures carried by circulating EVs.

DISCUSSION

Despite improvements in access to care and interventions, AP continues to be associated with significant morbidity and mortality. The timely and accurate diagnosis of AP and exact discrimination of MAP and SAP are still challenging but essential to change the situation.[35] The presented RAPIDx allows a fast EV isolation step from plasma samples via EXODUS within 15 min followed by high-throughput MALDI-TOF-MS detection of AP in 1 min, which may serve as a promising tool for AP precision diagnosis toward clinical translation.

EV proteomic applications demonstrate potential for biomarker discovery, which are close to being used for clinical translation.[36,37] In this study, the discovery of protein biosignatures with bottom-up proteomics using a high-resolution orbitrap allows us to detect 479 proteins from plasma EV samples, much more than the traditional proteomics method for a similar analysis (279 proteins).[38] The tedious sample preparation steps in bottom-up proteomics limit clinical translations, which require fast and accurate marker detection to ensure the patients receive timely treatments. MALDI-TOF MS is high throughput and rapid and is clinically suitable for fast large-scale proteomics and imaging studies.[39] Thus, applying bottom-up proteomics for biosignature screening and then using the integrated RAPIDx for marker cross-validation and detection is practically feasible for solving the unmet clinical needs of AP precision diagnosis.

Profiling and tracking EV proteins *via* bottom-up proteomics show close phenotype relationships between circulating EVs and multiple tissues and cells based on their specific proteomes (Figure 2b–c). This strongly supports the point that biomarker investigation from circulating EVs may provide potential insights for AP diagnosis, which also includes vital information for understanding the etiology and pathogenesis of AP and promotes biomarker discovery. Both bottom-up proteomics and MALDI-TOF analysis pointed out that the SAA proteins were significant biosignatures of AP. The SAA protein family comprises two main isoforms, SAA1 and SAA2, and they are acute-phase proteins and highly expressed in response to inflammation and tissue injury.[40] Their upregulation in the circulating EV is thought to be highly relevant to tissue inflammation during AP. We reasoned that using two different technologies raises the reliability and that findings replicated with two other groups of clinical samples are likely to be robust. It is worth mentioning that the SAA proteins are also the currently widely used serum biomarkers for AP diagnostics.[1,41] SAA1 expressed on circulating EVs has been characterized previously.[28] Here, we find that SAA expression levels (including SAA1 and SAA2) of plasma EVs were significantly characterized up-regulated in the AP group compared to the HC group. Notably, we further characterized that the different SAA isoforms expressed on EVs show diverse discriminatory power toward AP detection (Figure 3j–m, Figure 4e), reflecting that diagnosing AP from the detection of each isoform instead of total SAA proteins might help improve accuracy and specificity as each protein isoform may represent specific function pathologically.[42]

The protein fingerprints of intact EVs by MALDI-TOF tend to detect small protein ions (<20 kDa), so not all differential proteins from label-free proteomics were detected by integrated RAPIDx. The decreasing plasma FN1 has been seen in animals following the infusion of pancreatic proteases.[43,44] CD14 is a pattern-recognition receptor for several microbial products expressed on neutrophils and monocytes/macrophages. The circulating CD14-positive M2 monocytes have been reported to be associated with the severity of severe acute pancreatitis in Chinese patients.[45] DEFA1 has also been reported to relate to disease severity in COVID-19 patients.[46] It should be mentioned that S100A9 was a characteristic AP protein crossly identified by bottom-up proteomics and MALDI detection (Figure S5, Figure S9). The exosomal S100A9 has been involved in exosome-dependent NADPH oxidase activation, generating free radicals and promoting an inflammatory response during acute pancreatitis.[38] These differential proteins were shown to be carried by plasma EVs and may, to some extent, reflect the severity of AP development.

CONCLUSIONS

In conclusion, our work reveals that circulating EVs have close phenotype relationships to multiple tissues and cells, providing solid biological evidence for using EVs as potential biomarkers for disease detection. Based on this, we present a RAPIDx method for the precision diagnosis of AP based on the differentially expressed proteins carried by circulating EVs. We have included 115 clinical samples and discovered that plasma EVs differentially express SAA proteins that can be harnessed as potential biosignatures for AP detection with excellent AUCs ~ 97%. The SAA proteins can be further harnessed for discriminating AP severity with an AUC of 83%. This rapid, high-throughput, and high-sensitive detection method is critical for improving diagnostic efficiency and accuracy and eventually reducing the mortality of AP, pancreatic cancer, and other diseases.

METHODS

Clinical Sample Collection. The recruitment of patients was according to the Guidelines of the Declaration of Helsinki (Ethical Principles for Medical Research Involving Human Subjects, World Medical Association), following a protocol approved by the Institutional Review Board of the First Affiliated Hospital of Wenzhou Medical University (Wenzhou, China). The bottom-up proteomic

https://doi.org/10.1021/acsnano.3c00922
ACS Nano XXXX, XXX, XXX–XXX

analysis of EVs included HC (n = 15), MAP (n = 15), and SAP (n = 20) groups. In each group, the plasma samples were further prepared into 3, 3, and 4 sample pools for LC-MS analysis, respectively. The MALDI-TOF analysis included the following patients: HC (n = 36), MAP (n = 28), and SAP (n = 29). There were 28 shared samples between the proteomic study and MALDI-TOF analysis. The detailed clinical information is summarized in Table S1. All samples were collected when the patients were diagnosed before the treatments. The plasma sample was collected by centrifugation at 1500g for 20 min (two cycles) and stored at −80 °C until further use.

EV Isolation and Purification. For the bottom-up proteomic study, 200 μL of each plasma sample was diluted with phosphate buffered saline (1×PBS) to a final volume of 15 mL and then filtered by a 0.22 μm membrane filter (FPE-204-030, JET BIOFIL, Guangzhou, China) to exclude large particles and aggregates. The EV isolation was conducted by EXODUS according to our previously published method.[23] The 25 mm-diameter AAO (anodic aluminum oxide) membranes (Whatman, 20 nm in pore size) were applied, and the EV product was resuspended in 300 μL of PBS. For MALDI-TOF MS detection, 20 μL of plasma sample was diluted with PBS to a final volume of 5 mL and then filtered with a 0.22 μm membrane filter (FPE-204-013, JET BIOFIL, Guangzhou, China). Afterward, the plasma EV was isolated by the EXODUS equipped with 13 mm-diameter AAO membranes (Whatman, 20 nm in pore size). The purified EV product was resuspended in 200 μL PBS and stored at −80 °C until use.

Western Blotting Analysis. The protein concentrations were measured with a spectrophotometer (Nanodrop 2000, Thermo Fisher Scientific, USA). The electrophoretic separation of EV proteins was conducted by sodium dodecyl sulfate-polyacrylamide gel electrophoresis (SDS-PAGE), which was then transferred onto polyvinylidene fluoride (PVDF) membranes (10600023, GE Healthcare Life Science, Freiburg, Germany) for blotting analysis. The membrane was further blocked with 5% nonfat milk solution for 1 h at room temperature, and then was incubated with the primary antibody solution (1:1000 dilution) overnight at 4 °C. The following primary antibodies were applied: anti-Mac-2BP (sc-374541, Santa Cruz Biotechnology, Inc.), anti-flottilin1 (610821, BD, USA.), anti-CD9 (sc-13118, Santa Cruz Biotechnology, Inc.). After washing with PBST (PBS with 0.01% Tween 20), the membrane was incubated with the secondary antibody (7076S, Cell Signaling Technology) for 1 h. The images were visualized using the JS-M8 luminescence image analyzer (JS-M8, Pei Qing Science & Technology, Shanghai, China).

Nanoparticle Tracking Analysis (NTA). The EV concentrations and particle distributions were quantified by Nano Sight NS300 (Malvern) equipped with a 488 nm laser and a high-sensitivity sCMOS camera. The samples were appropriately diluted to achieve a particle per frame value of 20−50 for optimal counting. The camera level was set at 15. Each sample was measured 3 times, and the camera capture time was set at 30 s. All measurements were performed under identical conditions to ensure consistent results.

Transmission Electron Microscopy (TEM). The purified EV particles were fixed with 4% paraformaldehyde, then transported onto a Formvar/carbon-coated grid and allowed to sit for 30 min at room temperature. After that, the grid was washed with PBS (1×) 1 time, then placed into 1% glutaraldehyde for 5 min, followed by a wash step using double distilled water 4 times. Subsequently, the vesicles were negatively stained by a 1.5% uranyl acetate solution (v/v) for 45 s. After air-drying, the EV morphology was observed with a transmission electron microscope (Talos F200S, Thermo).

Immunoelectron Microscopy. First, the fixed EV particles (by 4% paraformaldehyde) were adsorbed onto carbon/Formvar-coated grids for 30 min for immunoelectron microscopy. The grids were washed with 50 mM glycine to remove free aldehyde groups. Next, the grids were blocked by 5% BSA solution for 1 h, then immediately conjugated to the primary antibody (anti-SAA sc-59679, Santa Cruz Biotechnology, Inc.) with a 1:200 dilution at 4 °C overnight. A grid without the primary antibody was prepared as a control sample. Afterward, the grids were rinsed with 0.1% BSA and then incubated with the secondary antibody (G7777, Sigma, Shanghai, China) for 2 h at room temperature. After incubation, the grids were washed with PBS and placed into 1% glutaraldehyde for 5 min. Next, the grids were washed with the double distilled water 4 times. After air-drying, the EV particles were stained with 1.5% uranyl acetate (v/v) for TEM imaging.

Bottom-Up Proteomic Analysis. EV proteomic analysis was performed using UPLC-MS/MS. The membranes of vesicles were disrupted by sonication with the addition of 1% protease inhibitor, and the obtained EV proteins were quantified using a BCA kit. An equal number of proteins from each sample was used for enzymatic hydrolysis to obtain peptides. Five mM of dithiothreitol (DTT, Promega) was added to the protein sample, and the incubation was carried out at 56 °C for 30 min. Then, 11 mM of iodoacetamide (IAA) was added to the sample and incubated for 15 min at room temperature in the dark. After that, trypsin was used to digest proteins at a ratio of 1:50 (protease: protein, m/m) overnight. The protein sample was further treated with trypsin at a ratio of 1:100 (protease: protein, m/m) to continue hydrolysis for 4 h. Finally, the digested sample was vacuum-dried and reconstituted in the mobile phase A, then separated using the EASY-nLC 1200 ultrahigh performance liquid system.

Mobile phase A comprises 0.1% formic acid and 2% acetonitrile; mobile phase B is an aqueous solution containing 0.1% formic acid and 90% acetonitrile. Liquid gradient setting: 0−68 min, 6%−23% B; 68−82 min, 23%−32% B; 82−86 min, 32−80% B; 86−90 min, 80% B. The flow rate is maintained at 500 nL/min. The separated peptides were injected into the NSI ion source for ionization and then entered the Orbitrap Exploris 480 mass spectrometer for analysis. The ion source voltage was set to 2.3 kV, and the FAIMS compensation voltages (CV) were −45 V and −65 V. The peptide precursor ions and their secondary fragments were detected and analyzed by a high-resolution Orbitrap. The data acquisition mode was the data-dependent scanning (DDA) program. For protein identification, the database was searched using Proteome Discoverer v2.1 (Thermo Fisher Scientific) with a 1% false discovery rate (FDR). The searched database was the Homo_SP_20201214.fasta database. Enrichment analysis was completed by http://metascape.org/.

Protein Tracking Analysis. The tracking analysis of circulating EV proteins was performed based on the detected proteins from the bottom-up proteomics (LC-MS/MS). The mapping of tissue/cell profiles was conducted using the specific proteome of tissues/cells described at Human Protein Atlas (https://www.proteinatlas.org), in which the protein expression data are from normal human tissue types derived from antibody-based protein profiling using immunohistochemistry. The number of mapped proteins in circulating EVs was counted for tissue/cell tracking analysis.

MALDI-TOF MS Analysis. EVs isolated by EXODUS were analyzed by an auto flex max MALDI-TOFLT (Bruker Daltonics) benchtop instrument for determining their fingerprints. The same amount of EVs for each sample was placed onto the target plated (MSP 96 target ground steel, Bruker Daltonics, Germany) and then vacuum-dried with a CentriVap Benchtop Vacuum Concentrator (Labconco, Kansas City, MO) at room temperature. The matrix used for sample preparation was the saturated 4-hydroxy-α-cyanocinnamic acid solution, prepared in 50% acetonitrile plus 0.1% trifluoroacetic acid. The resultant data were exported upon completion, and the spectra were then analyzed by ClinProTools 3.0 software (Bruker Daltonik). We used the Genetic Algorithm (GA) method for building a comparison model. The spectra were edited by Adobe Illustrator (Adobe Systems Incorporated, San Jose, CA).

Statistical Analysis. Data represented the mean ± SD of triplicate determinations from three independent experiments. Figures were edited by Adobe Illustrator (Adobe Systems Incorporated, San Jose, CA). Statistical analyses were performed by GraphPad Prism 7.0 (GraphPad Software, San Diego, CA). The heatmaps were made by TBtools (Version 3). Data were analyzed using a two-tailed Student's t test to compare the two groups. Differences were considered statistically significant when the P-value < 0.05.

https://doi.org/10.1021/acsnano.3c00922
ACS Nano XXXX, XXX, XXX−XXX

ASSOCIATED CONTENT

Supporting Information

The Supporting Information is available free of charge at https://pubs.acs.org/doi/10.1021/acsnano.3c00922.

Supporting figures for EV characterizations, EV protein tracking analysis, enrichment analysis and marker evaluations, supporting Table S1 of detailed clinical information (PDF)

Table S2: Proteins identified via bottom-up proteomics (XLSX)

Table S3: Peaks identified in fingerprints from the HC group and AP group (XLSX)

Table S4: Peaks identified in fingerprints from the MAP group and SAP group (XLSX)

AUTHOR INFORMATION

Corresponding Authors

Luke P. Lee − *Harvard Medical School, Department of Medicine, Brigham Women's Hospital, Boston, Massachusetts 02115, United States; Department of Bioengineering, Department of Electrical Engineering and Computer Science, University of California at Berkeley, Berkeley, California 94720, United States; Department of Biophysics, Institute of Quantum Biophysics, Sungkyunkwan University, Suwon, Gyeonggi-do 16419, Korea;* orcid.org/0000-0002-1436-4054; Email: lplee@bwh.harvard.edu

Fei Liu − *The First Affiliated Hospital of Wenzhou Medical University, Wenzhou, Zhejiang 325035, China; School of Ophthalmology & Optometry, School of Biomedical Engineering, Wenzhou Medical University, Wenzhou, Zhejiang 325035, China;* orcid.org/0000-0001-5259-5753; Email: feiliu@wmu.edu.cn

Authors

Qingfu Zhu − *National Engineering Research Center of Ophthalmology and Optometry, Eye Hospital, Wenzhou Medical University, Wenzhou 325027, China; School of Ophthalmology & Optometry, School of Biomedical Engineering, Wenzhou Medical University, Wenzhou, Zhejiang 325035, China;* orcid.org/0000-0003-1065-0739

Jiaxin Luo − *National Engineering Research Center of Ophthalmology and Optometry, Eye Hospital, Wenzhou Medical University, Wenzhou 325027, China; School of Ophthalmology & Optometry, School of Biomedical Engineering, Wenzhou Medical University, Wenzhou, Zhejiang 325035, China*

Hui-Ping Li − *The First Affiliated Hospital of Wenzhou Medical University, Wenzhou, Zhejiang 325035, China*

Wen Ye − *The First Affiliated Hospital of Wenzhou Medical University, Wenzhou, Zhejiang 325035, China*

Reguang Pan − *The First Affiliated Hospital of Wenzhou Medical University, Wenzhou, Zhejiang 325035, China*

Ke-Qing Shi − *The First Affiliated Hospital of Wenzhou Medical University, Wenzhou, Zhejiang 325035, China*

Rui Yang − *National Engineering Research Center of Ophthalmology and Optometry, Eye Hospital, Wenzhou Medical University, Wenzhou 325027, China; School of Ophthalmology & Optometry, School of Biomedical Engineering, Wenzhou Medical University, Wenzhou, Zhejiang 325035, China*

Hao Xu − *National Engineering Research Center of Ophthalmology and Optometry, Eye Hospital, Wenzhou Medical University, Wenzhou 325027, China; School of Ophthalmology & Optometry, School of Biomedical Engineering, Wenzhou Medical University, Wenzhou, Zhejiang 325035, China*

Hengrui Li − *National Engineering Research Center of Ophthalmology and Optometry, Eye Hospital, Wenzhou Medical University, Wenzhou 325027, China; School of Ophthalmology & Optometry, School of Biomedical Engineering, Wenzhou Medical University, Wenzhou, Zhejiang 325035, China*

Complete contact information is available at: https://pubs.acs.org/10.1021/acsnano.3c00922

Author Contributions

#Q. Zhu, J. Luo, Hui-Ping Li, and W. Ye contributed equally to this work. L. Lee and F. Liu conceived the project and designed the experiments. K. Shi and H. Li (Hui-ping Li) collected and analyzed the clinical samples. Q. Zhu, J. Luo, W. Ye, R. Pan, R. Yang, H. Xu, and H. Li (Hengrui Li) processed the whole experiment. Q. Zhu, J. Luo, and W. Ye prepared the manuscript and figures. L. Lee and F. Liu edited the manuscript. All experiments were conducted under the supervision of L. Lee and F. Liu. All authors have read and approved the final manuscript.

Notes

The authors declare no competing financial interest.

ACKNOWLEDGMENTS

The work was primarily supported by a research fund provided by the Zhejiang Provincial Natural Science Foundation (LY22H120002, LY20H150005), the Zhenan Technology City Research Fund, the National Natural Science Foundation of China (82241031 and 81800567), the Zhejiang Provincial and Ministry of Health Research Fund for Medical Sciences (WKJ-ZJ-1910), the Wenzhou Medical University (89218012), and the Wenzhou Basic Research Projects (Y2020916).

REFERENCES

(1) Shah, A. P.; Mourad, M. M.; Bramhall, S. R. Acute Pancreatitis: Current Perspectives on Diagnosis and Management. *J. Inflamm. Res.* **2018**, *11*, 77−85.

(2) Sun, H.; Zuo, H. D.; Lin, Q.; Yang, D. D.; Zhou, T.; Tang, M. Y.; Wáng, Y. X. J.; Zhang, X. M. Mr Imaging for Acute Pancreatitis: The Current Status of Clinical Applications. *Ann. Transl. Med.* **2019**, *7*, 269.

(3) Afghani, E.; Pandol, S. J.; Shimosegawa, T.; Sutton, R.; Wu, B. U.; Vege, S. S.; Gorelick, F.; Hirota, M.; Windsor, J.; Lo, S. K.; Freeman, M. L.; Lerch, M. M.; Tsuji, Y.; Melmed, G. Y.; Wassef, W.; Mayerle, J. Acute Pancreatitis-Progress and Challenges: A Report on an International Symposium. *Pancreas* **2015**, *44*, 1195−1210.

(4) Garg, P. K.; Singh, V. P. Organ Failure Due to Systemic Injury in Acute Pancreatitis. *Gastroenterology* **2019**, *156*, 2008−2023.

(5) Mederos, M. A.; Reber, H. A.; Girgis, M. D. Acute Pancreatitis: A Review. *Jama* **2021**, *325*, 382−390.

(6) Zhou, Y.; Ge, Y.-t.; Shi, X.-l.; Wu, K.-y.; Chen, W.-w.; Ding, Y.-b.; Xiao, W.-m.; Wang, D.; Lu, G.-t.; Hu, L.-h. Machine Learning Predictive Models for Acute Pancreatitis: A Systematic Review. *Int. J. Med. Inform.* **2022**, *157*, 104641.

(7) Möller, A.; Lobb, R. J. The Evolving Translational Potential of Small Extracellular Vesicles in Cancer. *Nat. Rev. Cancer* **2020**, *20*, 697−709.

(8) Whiteside, T. L. Validation of Plasma-Derived Small Extracellular Vesicles as Cancer Biomarkers. *Nat. Rev. Clin. Oncol.* **2020**, *17*, 719−720.
(9) Kalluri, R.; LeBleu, V. S. The Biology, Function, and Biomedical Applications of Exosomes. *Science* **2020**, *367*, No. eaau6977, DOI: 10.1126/science.aau6977.
(10) Bahram Sangani, N.; Gomes, A. R.; Curfs, L. M. G.; Reutelingsperger, C. P. The Role of Extracellular Vesicles During Cns Development. *Prog. Neurobiol.* **2021**, *205*, 102124.
(11) van Niel, G.; D'Angelo, G.; Raposo, G. Shedding Light on the Cell Biology of Extracellular Vesicles. *Nat. Rev. Mol. Cell Biol.* **2018**, *19*, 213−228.
(12) Cheng, L.; Hill, A. F. Therapeutically Harnessing Extracellular Vesicles. *Nat. Rev. Drug Discovery* **2022**, *21*, 379−399.
(13) Zhu, Q.; Huang, Y.; Yang, Q.; Liu, F. Recent Technical Advances to Study Metabolomics of Extracellular Vesicles. *Microchem. J.* **2021**, *171*, 106816.
(14) Jia, Y. C.; Ding, Y. X.; Mei, W. T.; Wang, Y. T.; Zheng, Z.; Qu, Y. X.; Liang, K.; Li, J.; Cao, F.; Li, F. Extracellular Vesicles and Pancreatitis: Mechanisms, Status and Perspectives. *Int. J. Biol. Sci.* **2021**, *17*, 549−561.
(15) Bonjoch, L.; Casas, V.; Carrascal, M.; Closa, D. Involvement of Exosomes in Lung Inflammation Associated with Experimental Acute Pancreatitis. *J. Pathol.* **2016**, *240*, 235−245.
(16) Liu, J.; Niu, Z.; Zhang, R.; Peng, Z.; Wang, L.; Liu, Z.; Gao, Y.; Pei, H.; Pan, L. Malat1 Shuttled by Extracellular Vesicles Promotes M1 Polarization of Macrophages to Induce Acute Pancreatitis Via Mir-181a-5p/Hmgb1 Axis. *J. Cell. Mol. Med.* **2021**, *25*, 9241−9254.
(17) Jiménez-Alesanco, A.; Marcuello, M.; Pastor-Jiménez, M.; López-Puerto, L.; Bonjoch, L.; Gironella, M.; Carrascal, M.; Abian, J.; de-Madaria, E.; Closa, D. Acute Pancreatitis Promotes the Generation of Two Different Exosome Populations. *Sci. Rep.* **2019**, *9*, 19887.
(18) Coumans, F. A.W.; Brisson, A. R.; Buzas, E. I.; Dignat-George, F.; Drees, E. E.E.; El-Andaloussi, S.; Emanueli, C.; Gasecka, A.; Hendrix, A.; Hill, A. F.; Lacroix, R.; Lee, Y.; van Leeuwen, T. G.; Mackman, N.; Mager, I.; Nolan, J. P.; van der Pol, E.; Pegtel, D. M.; Sahoo, S.; Siljander, P. R.M.; Sturk, G.; de Wever, O.; Nieuwland, R. Methodological Guidelines to Study Extracellular Vesicles. *Circ. Res.* **2017**, *120*, 1632−1648.
(19) Wang, Z.; Wang, H.; Becker, R.; Rufo, J.; Yang, S.; Mace, B. E.; Wu, M.; Zou, J.; Laskowitz, D. T.; Huang, T. J. Acoustofluidic Separation Enables Early Diagnosis of Traumatic Brain Injury Based on Circulating Exosomes. *Microsyst. Nanoeng.* **2021**, *7*, 20.
(20) Hao, N.; Wang, Z.; Liu, P.; Becker, R.; Yang, S.; Yang, K.; Pei, Z.; Zhang, P.; Xia, J.; Shen, L.; Wang, L.; Welsh-Bohmer, K. A.; Sanders, L. H.; Lee, L. P.; Huang, T. J. Acoustofluidic Multimodal Diagnostic System for Alzheimer's Disease. *Biosens. Bioelectron.* **2022**, *196*, 113730.
(21) Abreu, C. M.; Costa-Silva, B.; Reis, R. L.; Kundu, S. C.; Caballero, D. Microfluidic Platforms for Extracellular Vesicle Isolation, Analysis and Therapy in Cancer. *Lab Chip* **2022**, *22*, 1093−1125.
(22) Jin, G.; Hong, S.; Rich, J.; Xia, J.; Kim, K.; You, L.; Zhao, C.; Huang, T. J. Intelligent Nanoscope for Rapid Nanomaterial Identification and Classification. *Lab Chip* **2022**, *22*, 2978−2985.
(23) Chen, Y.; Zhu, Q.; Cheng, L.; Wang, Y.; Li, M.; Yang, Q.; Hu, L.; Lou, D.; Li, J.; Dong, X.; Lee, L. P.; Liu, F. Exosome Detection Via the Ultrafast-Isolation System: Exodus. *Nat. Methods* **2021**, *18*, 212−218.
(24) Szaejli, E.; Feheer, T.; Medzihradszky, K. F. Investigating the Quantitative Nature of Maldi-Tof Ms. *Mol. Cell Proteomics.* **2008**, *7*, 2410−2418.
(25) Kim, S.; Ruparel, H. D.; Gilliam, T. C.; Ju, J. Digital Genotyping Using Molecular Affinity and Mass Spectrometry. *Nat. Rev. Genet.* **2003**, *4*, 1001−1008.
(26) Fournier, P.-E.; Drancourt, M.; Colson, P.; Rolain, J.-M.; Scola, B. L.; Raoult, D. Modern Clinical Microbiology: New Challenges and Solutions. *Nat. Rev. Microbiol.* **2013**, *11*, 574−585.
(27) Zhu, Y.; Pick, H.; Gasilova, N.; Li, X.; Lin, T.-E.; Laeubli, H. P.; Zippelius, A.; Ho, P.-C.; Girault, H. H. Maldi Detection of Exosomes: A Potential Tool for Cancer Studies. *Chem.* **2019**, *5*, 1318−1336.
(28) Zheng, H.; Zhao, J.; Wang, X.; Yan, S.; Chu, H.; Gao, M.; Zhang, X. Integrated Pipeline of Rapid Isolation and Analysis of Human Plasma Exosomes for Cancer Discrimination Based on Deep Learning of Maldi-Tof Ms Fingerprints. *Anal. Chem.* **2022**, *94*, 1831−1839.
(29) Han, Z.; Yi, J.; Yang, Y.; Li, D.; Peng, C.; Long, S.; Peng, X.; Shen, Y.; Liu, B.; Qiao, L. Sers and Maldi-Tof Ms Based Plasma Exosome Profiling for Rapid Detection of Osteosarcoma. *Analyst* **2021**, *146*, 6496−6505.
(30) Ye, W.; Pan, R.; Shi, K.-Q.; Li, H.-P.; Lee, L. P.; Liu, F. Isolation of Small Extracellular Vesicles from a Drop of Plasma Via Exodus and Their Fingerprint Proteomics Profiling by Maldi-Tof Ms. *Biosens. Bioelectro.: X* **2022**, *10*, 100099.
(31) Théry, C.; Witwer, K. W.; Aikawa, E.; Alcaraz, M. J.; Anderson, J. D.; Andriantsitohaina, R.; Antoniou, A.; Arab, T.; Archer, F.; Atkin-Smith, G. K.; Ayre, D. C.; Bach, J.-M.; Bachurski, D.; Baharvand, H.; Balaj, L.; Baldacchino, S.; Bauer, N. N.; Baxter, A. A.; Bebawy, M.; Beckham, C.; et al. Minimal Information for Studies of Extracellular Vesicles 2018 (Misev2018): A Position Statement of the International Society for Extracellular Vesicles and Update of the Misev2014 Guidelines. *J. Extracell. Vesicles* **2018**, *7*, 1535750.
(32) Zhang, X.; Li, Z.; Liu, W.; Du, J.; Liu, Y.; Yu, N.; Liu, C.; Zeng, M.; Zhang, X. The Complement and Coagulation Cascades Pathway Is Associated with Acute Necrotizing Pancreatitis by Genomics and Proteomics Analysis. *J. Inflamm. Res.* **2022**, *15*, 2349−2363.
(33) Gao, J.; Meyer, K.; Borucki, K.; Ueland, P. M. Multiplex Immuno-Maldi-Tof Ms for Targeted Quantification of Protein Biomarkers and Their Proteoforms Related to Inflammation and Renal Dysfunction. *Anal. Chem.* **2018**, *90*, 3366−3373.
(34) Milan, E.; Lazzari, C.; Anand, S.; Floriani, I.; Torri, V.; Sorlini, C.; Gregorc, V.; Bachi, A. Saa1 Is over-Expressed in Plasma of Non Small Cell Lung Cancer Patients with Poor Outcome after Treatment with Epidermal Growth Factor Receptor Tyrosine-Kinase Inhibitors. *J. Proteomics* **2012**, *76*, 91−101.
(35) Greenberg, J. A.; Hsu, J.; Bawazeer, M.; Marshall, J.; Friedrich, J. O.; Nathens, A.; Coburn, N.; May, G. R.; Pearsall, E.; McLeod, R. S. Clinical Practice Guideline: Management of Acute Pancreatitis. *Can. J. Surg.* **2016**, *59*, 128−140.
(36) Bandu, R.; Oh, J. W.; Kim, K. P. Mass Spectrometry-Based Proteome Profiling of Extracellular Vesicles and Their Roles in Cancer Biology. *Exp. Mol. Med.* **2019**, *51*, 1−10.
(37) Zhu, Q.; Xu, H.; Huang, L.; Luo, J.; Li, H.; Yang, R.; Liu, X.; Liu, F. Identification and Detection of Plasma Extracellular Vesicles-Derived Biomarkers for Esophageal Squamous Cell Carcinoma Diagnosis. *Biosens. Bioelectron.* **2023**, *225*, 115088.
(38) Carrascal, M.; Areny-Balagueró, A.; de-Madaria, E.; Cárdenas-Jaén, K.; García-Rayado, G.; Rivera, R.; Martin Mateos, R. M.; Pascual-Moreno, I.; Gironella, M.; Abian, J.; Closa, D. Inflammatory Capacity of Exosomes Released in the Early Stages of Acute Pancreatitis Predicts the Severity of the Disease. *J. Pathol.* **2022**, *256*, 83−92.
(39) Singhal, N.; Kumar, M.; Kanaujia, P. K.; Virdi, J. S. Maldi-Tof Mass Spectrometry: An Emerging Technology for Microbial Identification and Diagnosis. *Front. Microbiol.* **2015**, *6*, 791.
(40) Sack, G. H., Jr. Serum Amyloid a (Saa) Proteins. *Subcell. Biochem.* **2020**, *94*, 421−436.
(41) Stirling, A. D.; Moran, N. R.; Kelly, M. E.; Ridgway, P. F.; Conlon, K. C. The Predictive Value of C-Reactive Protein (Crp) in Acute Pancreatitis - Is Interval Change in Crp an Additional Indicator of Severity? *HPB* **2017**, *19*, 874−880.
(42) Soler, L.; Luyten, T.; Stinckens, A.; Buys, N.; Cerón, J. J.; Niewold, T. A. Serum Amyloid A3 (Saa3), Not Saa1 Appears to Be the Major Acute Phase Saa Isoform in the Pig. *Vet. Immunol. Immunop.* **2011**, *141*, 109−115.
(43) Bellows, C. F.; Brain, J. D. Role of Fibronectin in Pancreatitis-Associated Lung Injury. *Dig. Dis. Sci.* **2003**, *48*, 1445−1452.

https://doi.org/10.1021/acsnano.3c00922
ACS Nano XXXX, XXX, XXX−XXX

(44) Cohler, L. F.; Saba, T. M.; Lewis, E. P. Lung Vascular Injury with Protease Infusion. Relationship to Plasma Fibronectin. *Ann. Surg.* **1985**, *202*, 240−247.
(45) Zhang, M.; Ding, L.; Wang, X.; Hou, J.; Li, M.; Jiang, Y.; He, X.; Cui, M.; Hu, F.; Zhang, X.; Yang, J.; Guo, X.; Zhao, H.; Gao, P. Circulating Cd14(+)Cd163(+)Cd115(+) M2Monocytes Are Associated with the Severity of New Onset Severe Acute Pancreatitis in Chinese Patients. *Int. Immunopharmacol.* **2018**, *57*, 181−189.
(46) Shrivastava, S.; Chelluboina, S.; Jedge, P.; Doke, P.; Palkar, S.; Mishra, A. C.; Arankalle, V. A. Elevated Levels of Neutrophil Activated Proteins, Alpha-Defensins (Defa1), Calprotectin (S100a8/A9) and Myeloperoxidase (Mpo) Are Associated with Disease Severity in Covid-19 Patients. *Front. Cell. Infect. Microbiol.* **2021**, *11*, 751232−751232.

https://doi.org/10.1021/acsnano.3c00922
ACS Nano XXXX, XXX, XXX−XXX